JOURNAL OF THE MECHANICAL BEHAVIOR OF BIOMEDICAL MATERIALS 4 (2011) 1764–1773

Available online at www.sciencedirect.com

SciVerse ScienceDirect

journal homepage: www.elsevier.com/locate/jmbbm

Research paper

Fracture characterization of bone under mode II loading using the end loaded split test

F.A.M. Pereira[a], J.J.L. Morais[a], N. Dourado[a], M.F.S.F. de Moura[b,*], M.I.R. Dias[c]

[a] CITAB/UTAD, Departamento de Engenharias, Quinta de Prados, 5001-801 Vila Real, Portugal
[b] Faculdade de Engenharia da Universidade do Porto, Departamento de Engenharia Mecânica, Rua Dr. Roberto Frias, 4200-465 Porto, Portugal
[c] UTAD, Departamento de Ciências Veterinárias, Quinta de Prados, 5001-801 Vila Real, Portugal

ARTICLE INFO

Article history:
Received 25 February 2011
Received in revised form
17 May 2011
Accepted 28 May 2011
Published online 6 June 2011

Keywords:
Bone
Fracture characterization
Mode II
End loaded split test

ABSTRACT

Fracture energy release rate under mode II loading of bovine cortical bone is determined using a miniaturized testing device of the end loaded split test. The energy release rate is evaluated by means of a data reduction scheme based on specimen compliance, beam theory and crack equivalent concept. Experimental tests were carried out to evaluate the *Resistance* curve which provides a successful method to characterize fracture behavior of quasi-brittle materials like bone. A numerical analysis including a cohesive damage model was used to validate the procedure. It was demonstrated that the end loaded split test and proposed data reduction scheme provide a valuable solution for mode II fracture characterization of bone.

1. Introduction

The study of bone fracture is an important research topic since it can contribute to understanding the fundamentals of bone failure induced by disease, age, drugs and exercise. In fact, fracture mechanics measurements can be viewed as a valuable method to characterize the toughness of bone, providing a quantitative determination of its fracture resistance. In this context, the definition of appropriate testing methods to evaluate fracture properties of bone is fundamental. However, classical fracture tests used for other materials require special adaptations owing to bone characteristics. Effectively, bone can be viewed as a natural composite material mainly constituted by an inorganic (mineral) phase (hydroxyapatite), collagen fibers and water, organized in a highly anisotropic and heterogeneous microstructure. The mineral phase is essentially responsible for stiffness and strength while the organic phase (collagen) and water play an essential role on toughness (Hernandez et al., 2001; Wang et al., 2002; Morais et al., 2010). As a consequence of its microstructure and of interaction between its constituents, fracture of bone reveals some toughening mechanisms in the vicinity of the crack tip, like micro-cracking, crack deflection and fiber bridging (Zioupos, 1998; Nalla et al., 2003). These mechanisms are responsible for the development of a non-negligible fracture process zone (FPZ), which means that linear elastic fracture mechanics (LEFM) theory does not apply. In this case, the best method

* *Corresponding author.* Tel.: +351 225 081 727; fax: +351 225 081 584.
E-mail address: mfmoura@fe.up.pt (M.F.S.F. de Moura).

1751-6161/$ - see front matter © 2011 Elsevier Ltd. All rights reserved.
doi:10.1016/j.jmbbm.2011.05.033

to determine bone toughness is by means of the *Resistance* curve (*R* curve) which describes the evolution of the fracture energy as a function of damage progression. An additional difficulty is related to limitations on specimen dimensions that are possible to be harvested from bone. These aspects restrict the definition of adequate tests to analyze fracture characteristics of bone.

The majority of studies found in the literature are dedicated to bone mode I fracture. The compact tension test (Norman et al., 1995) and the single-edge notched specimen under three point bending (Phelps et al., 2000) are the most used. However, these tests present a limitation related to the confinement of the non-negligible FPZ induced by compressive stresses that develop ahead of the crack tip due to bending (de Moura et al., 2010a; Dourado et al., 2011). This is a spurious phenomenon that can artificially increase the measured toughness and lead to overestimation of bone fracture properties. Since bone specimens have obvious limitations in size, this kind of difficulty arises naturally. Morais et al. (2010) have recently proposed the miniaturized double cantilever beam (DCB) test that allows us to overcome these drawbacks. In this work, the authors proposed a smaller version of the traditional DCB specimen owing to size restrictions imposed by bovine bone femur dimensions. As the DCB specimen propitiates a longer length for self-similar crack propagation without undertaking the influence of spurious effects, an *R* curve was obtained allowing an adequate characterization of bone fracture under pure mode I loading.

Much less attention has been dedicated to mode II fracture in bone. The fundamental reasons are related to experimental difficulties, namely the definition of an appropriate test method. However, fracture characterization under mode II acquires special relevance for different reasons. Effectively, fractures can occur under pure shear loading, as is the case of twisting or torsion efforts during normal activities (Turner et al., 2001). Additionally, mixed-mode fracture conditions involving modes I and II will prevail under general loading. Moreover, mixed-mode fracture conditions are also stimulated by bone anisotropy which defines directions prone to failure. In fact, the pronounced anisotropy induced by alignment of osteons along the long axis of bone delineates regions prone to define crack propagation paths. Consequently, cracks can initiate and propagate under mixed-mode conditions, since they are confined and obliged to grow in pre-established regions. Therefore, the definition of a fracture envelope in mode I versus mode II space is a fundamental task, which obviously reinforces the need of fracture characterization under pure mode II loading.

A possible solution to characterize fracture of human bone under mode II loading was pointed out by Norman et al. (1996) with the compact shear test. The proposed specimen has shown small sensitivity of compliance (*C*) as a function of crack length (*a*), which makes difficult the establishment of the compliance calibration function $C = f(a)$. In addition, the propagation is unstable which renders difficult the measurement of toughness in pure-mode II. Zimmermann et al. (2009, 2010) proposed an asymmetric four-point bending test using single edge notched specimens to fracture characterization of bone under mixed-mode I + II loading. The mode II is achieved when the pre-crack is aligned with the centerline of the rig, since in this case the bending moment vanishes and only a shear force is applied. de Moura et al. (2010b) have recently performed detailed numerical analyses using cohesive zone modeling on the application of the end loaded split (ELS) and end notched flexure (ENF) tests to pure mode II fracture characterization of bone. Considering typical ranges of bone properties the authors concluded that both tests can be used for this objective, with a judicious selection of the specimens' dimensions. However, the authors realized that the ELS test provides a longer extent with self-similar crack propagation, i.e., without spurious effects affecting the free development of FPZ. As a consequence of this statement the ELS test is used in the present work to characterize fracture behavior of cortical bovine bone under pure mode II loading. With this aim, a miniaturized testing device was designed in order to account for bone specificities, namely the available specimen size. An equivalent crack length method based on beam theory and specimen compliance was used to overcome the difficulties inherent to crack monitoring during its growth. The data reduction scheme provides the attainment of the *R* curve, which allows determining the extent of the FPZ and the critical fracture energy from its plateau. The method was numerically validated by means of cohesive zone modeling, which permits simulating damage initiation and growth. The data reduction method was subsequently applied with success to experimental results in order to evaluate mode II bone toughness. The main conclusion is that the proposed test (ELS) and data reduction scheme provide a simple, expeditious and adequate methodology to evaluate mode II fracture characteristics of bone. Alternative testing methods proposed in the literature were also studied numerically. Comparisons between the ELS test and those alternative solutions were performed and conclusions about their limitations are drawn.

2. Experiments

Ten specimens were prepared from fresh bovine femora of young animals (aged about 8 months) within one day post-mortem. During the specimens' machining process the endosteal and periosteal tissues were removed. Specimens were preserved with physiological saline at all steps of the machining process and frozen at −20 °C for storage. The initial crack length a_0 is constituted by a notch (0.3 mm thick) performed with a circular saw, and a small crack (0.25 mm length) executed with a sharp blade. This process usually reproduces natural cracks in a realistic way. This is an important issue since blunt pre-cracks induce unrealistic increase of fracture energy at crack starting advance (Morais et al., 2010). Nevertheless, as will be discussed later, the data reduction scheme used allows overcoming any imprecision on the execution of the pre-crack. As observed in Fig. 1, specimens were conceived in order to provide propagation in the TL fracture system (i.e., the normal to the crack plane is the tangential direction of mid-diaphysis and the crack propagation direction is the longitudinal direction of mid-diaphysis). Prior to the pre-crack execution the longitudinal

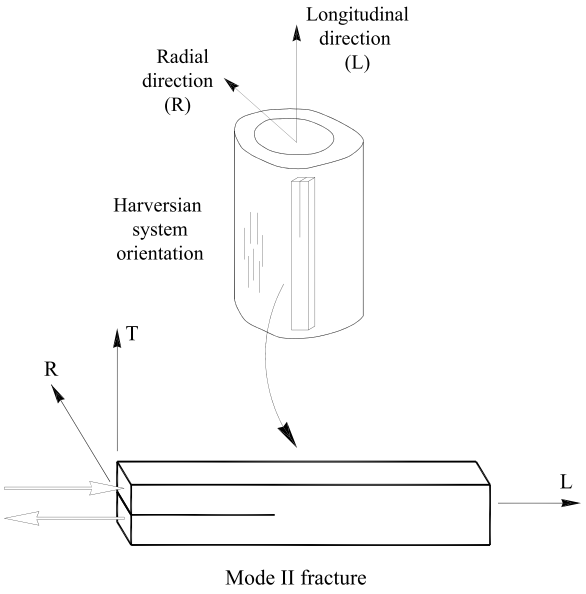

Fig. 1 – Schematic diagram of a bone femur showing the location where samples can be harvested.

modulus (E_L) was determined for each specimen before introducing the pre-crack, by means of the three-point bending test. Since the experimental praxis during the ELS tests revealed that crack frequently deviates from its initial plane ($z = 0$ in Fig. 2), two slight longitudinal grooves have been machined in each lateral side of the specimen to diminish the width (b instead of B in Fig. 2) of the ligament area, thus compelling crack advance to occur along the L-axis. Previous simulations (de Moura et al., 2010b) and preliminary fracture tests allowed the definition of adequate specimen nominal dimensions: $L_1 = 60, L = 50, d = 3, a_0 = 20, 2h = 6, b = 2.3, B = 3.3$ and $t = 1$ (dimensions in mm).

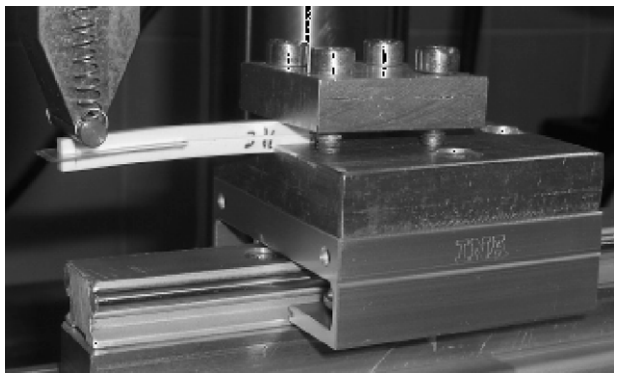

Fig. 3 – Testing setup for the ELS test.

Fracture tests were performed under displacement control (0.5 mm/min) using a servo-electrical material testing system (MicroTester INSTRON 5848), using a 2 kN load-cell, for an acquisition frequency of 5 Hz. During the test, the applied load (P) and displacement (δ) were registered. As observed in Fig. 3 the fixture testing device includes a linear guidance system which allows horizontal translation of the clamping grip during the loading process. This solution avoids tensile stress development along the longitudinal direction. Two thin Teflon® films with a pellicle of lubricator between them were introduced in the pre-crack region (Fig. 3) to reduce the friction effects (de Moura et al., 2009). One crucial aspect of this test is associated to the clamping conditions. In a recent numerical study (de Moura et al., 2010b) the effect of tightening was thoroughly analyzed. It was verified that a tightening of 0.1 mm provides satisfactory measurements of mode II toughness (G_{IIc}) without overcoming compressive strength of bone.

Fig. 4 shows the crack detail during propagation. Sliding at the notch tip (see the detail in Fig. 4) clearly demonstrates the

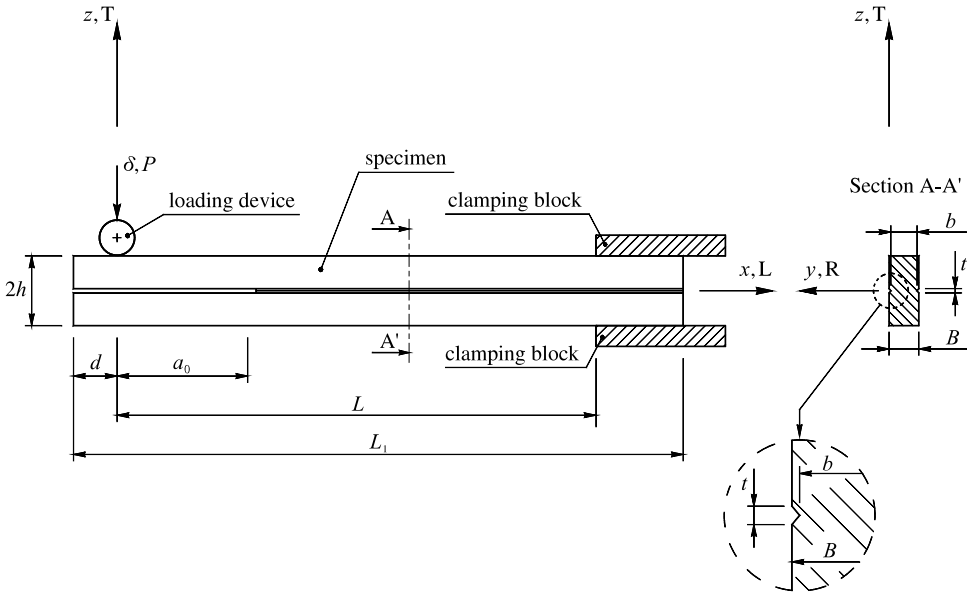

Fig. 2 – Schematic representation of the ELS test.

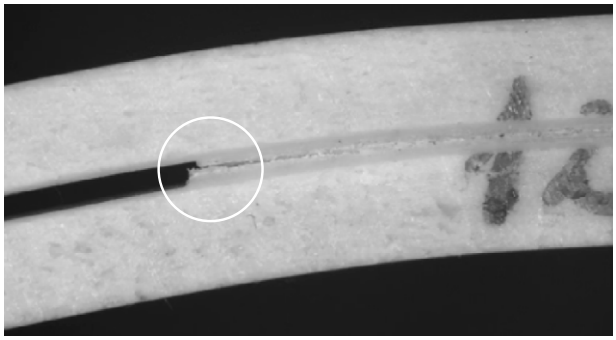

Fig. 4 – Specimen detail showing the relative displacement at the crack notch.

existence of a pure mode II loading. On the other hand, it is evident that the position of the crack tip is not undoubtedly identified with the necessary accuracy. As a result, the application of classical data reduction schemes based on crack length (a) monitoring during propagation can lead to miscalculations of fracture energy, due to errors committed on crack length measurements. To overcome this drawback an equivalent crack length based method is presented in the next section.

3. Crack equivalent based method

Mode II fracture energy is classically measured through the compliance calibration method (CCM) or by means of corrected beam theory (CBT). In regards to CCM, the energy release rate is evaluated through Irwin–Kies equation,

$$G_{II} = \frac{P^2}{2B}\frac{dC}{da} \tag{1}$$

which requires compliance ($C = \delta/P$) calibration during crack propagation, i.e., $C = f(a)$. Alternatively, CBT (Wang and Williams, 1992) can be used, through

$$G_{II} = \frac{9P^2(a + |\Delta_{II}|)^2}{4B^2h^3E_L} \tag{2}$$

with B standing for the specimen width, h for the specimen mid-height, E_L for the longitudinal elastic modulus, and Δ_{II} for a crack length correction accounting for shear and beam rotation effects ($\Delta_{II} = 0.49\,\Delta_I$), being

$$\Delta_I = h\sqrt{\frac{E_L}{11G_{LT}}\left[3 - 2\left(\frac{\Gamma}{1+\Gamma}\right)^2\right]} \tag{3}$$

with

$$\Gamma = 1.18\frac{\sqrt{E_L E_T}}{G_{LT}}. \tag{4}$$

Parameters E_T and G_{LT} are the transverse and shear modulus, respectively (Fig. 2). Both methods (i.e., CCM and CBT) require crack length monitoring, which is not easy to accomplish with the required accuracy, as discussed in the previous section (Fig. 4). To obviate this disadvantage a crack equivalent method based on current specimen compliance and beam theory is adopted. The equation of compliance as a function of crack length can be obtained by means of specimen elastic strain energy, considered as a clamped beam with a crack

$$U = \int_0^L \frac{M_f^2}{2E_L I}dx + \int_0^L\int_{-h}^{h}\frac{\tau^2}{2G_{LT}}B\,dz\,dx \tag{5}$$

where M_f and I stand for bending moment and second moment of area, respectively (Fig. 2). The shear stress τ is

$$\tau = \frac{3}{2}\frac{V_j}{A_j}\left(1 - \frac{z^2}{c_j^2}\right). \tag{6}$$

The parameters A_j, c_j and V_j represent, respectively, specimen cross-section area, beam half-thickness and transverse load acting on the segment j ($0 \le x \le a$ or $a \le x \le L$). Therefore, for a given crack length a, the Castigliano theorem (i.e., $\delta = dU/dP$) can be applied at the loading point, yielding

$$C - \frac{3a^3}{2Bh^3E_L} = \frac{L^3}{2Bh^3E_L} + \frac{3L}{5BhG_{LT}}. \tag{7}$$

In the ELS test there are two sources of variability from specimen to specimen. Effectively, bone being a natural material presents some scatter on its elastic properties, namely on its longitudinal modulus of elasticity (E_L), which means that a measurement of this elastic property must be performed for each specimen. On the other hand, it is recognized that real clamping conditions are never perfect. This issue influences the specimen behavior and is not accounted for in Eq. (7). It can be accounted for by considering an effective specimen length (L_{ef}) which, in fact, is the theoretical length that a specimen should present in order to satisfy Eq. (7). This parameter (L_{ef}) can be estimated using the initial (elastic) response of an experimental test (i.e., a_0 and C_0) in Eq. (7),

$$C_0 - \frac{3a_0^3}{2Bh^3E_L} = \frac{L_{ef}^3}{2Bh^3E_L} + \frac{3L_{ef}}{5BhG_{LR}}. \tag{8}$$

Combining Eqs. (7) and (8) the equivalent crack length (instead of a) during propagation becomes

$$a_e = \left[(C - C_0)\frac{2Bh^3E_L}{3} + a_0^3\right]^{1/3} \tag{9}$$

which does not depend on parameter L_{ef}. The strain energy release rate in mode II (G_{II}) can now be obtained from Eqs. (7), (9) and (1). It should be noted that due to the presence of longitudinal grooves (Fig. 2) the width of the ligament section is b, instead of B. Therefore,

$$G_{II} = \frac{9P^2a_e^2}{4bBh^3E_L}. \tag{10}$$

Following this methodology the mode II R curve is obtained as a function of a_e, and the critical fracture energy G_{IIc} is captured from its plateau. The method only requires the previous measurement of E_L as well as the load–displacement data obtained during the experimental test. Hence, the problem associated to crack length monitoring is surmounted, since the crack is a calculated parameter instead of a measured one. Additionally, this procedure allows accounting for the fracture process zone (FPZ) development. In fact, quasi-brittle materials like bone are characterized by a non-negligible FPZ which must be accounted for, since its presence affects fracture behavior. This is achieved by means of the proposed data reduction scheme, seeing that the FPZ influences specimen compliance which is used to get the R curve.

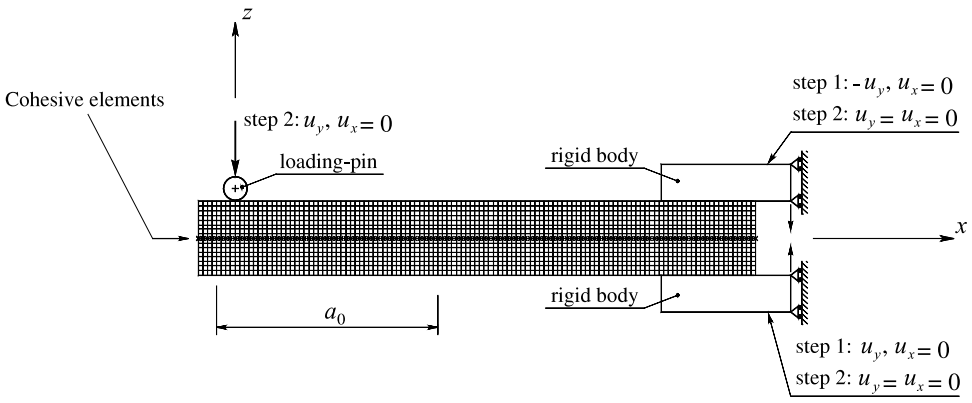

Fig. 5 – Finite element mesh used in the numerical simulations (ELS test). Diagonal crosses at the mid-thickness represent cohesive elements.

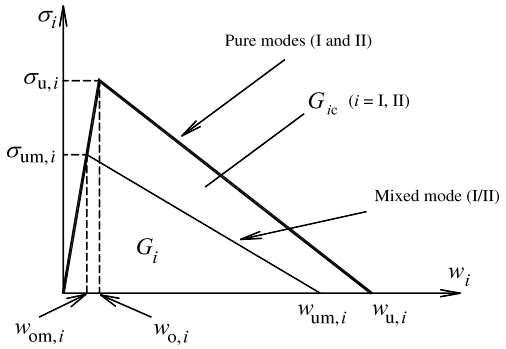

Fig. 6 – Sketch of pure (I or II) and mixed (I + II) bilinear cohesive model.

4. Model validation

In order to validate the proposed data reduction scheme (Section 3) a numerical analysis including cohesive zone modeling was performed. A two-dimensional plane stress analysis involving 7680 8-node solid elements (width B), and 240 6-node cohesive elements (width b) allowing us to simulate damage onset and propagation, was performed (Fig. 5). Following this strategy, the presence of the longitudinal grooves in the specimen is taken into account, given that the fracture section presents a width b instead of B (Fig. 2). Opened cohesive elements were considered in the pre-crack region in order to avoid interpenetration. These opened elements transmit normal compressive stresses and allow a free sliding between the crack surfaces. Since thin lubricated Teflon® films were introduced at the pre-crack, friction effects were neglected. The loading cylinder (Fig. 3) was simulated as a rigid body (Fig. 5) and contact conditions were considered to avoid interpenetration. Two rectangular rigid blocks were used to impose clamping conditions (step 1 in Fig. 5) by tightening the specimen (0.1 mm) prior to the load application, considering a friction coefficient of 0.25. Fracture was induced in the TL system imposing a vertical displacement (step 2: u_y in Fig. 5) to the loading-pin. Typical elastic properties of bovine cortical bone (Table 1) were used in the numerical model. A mixed-mode cohesive damage model was incorporated in the numerical analysis. A linear softening relationship between stresses and relative displacements (Fig. 6) is assumed to simulate a gradual material degradation during the loading process. The cohesive zone model establishes a relationship between stresses and relative displacements. In the initial linear region stresses are obtained from the product between the interfacial stiffness and relative displacements. Once the local strength ($\sigma_{u,i}$, $i = I, II$) is attained the initial interface stiffness is gradually reduced leading to a linear decrease of stresses. In pure mode model, the ultimate relative displacement $w_{u,i}$ ($i = I, II$) is defined equating the area circumscribed by the triangle to G_{ic} ($i = I, II$). Mixed-mode damage model is an extension of pure mode model. In this case, a quadratic stress criterion is utilized to simulate damage onset

Table 1 – Elastic properties of bovine cortical bone (Morais et al., 2010; Martin et al., 1998).

E_L (GPa)	E_T (GPa)	G_{LT} (GPa)	ν_T
19.94	11.7	4.1	0.36

$$\left(\frac{\sigma_I}{\sigma_{u,I}}\right)^2 + \left(\frac{\sigma_{II}}{\sigma_{u,II}}\right)^2 = 1 \quad \text{if } \sigma_I \geq 0$$
$$\sigma_{II} = \sigma_{u,II} \quad \text{if } \sigma_I \leq 0 \tag{11}$$

where σ_i represent the stresses in each mode and $\sigma_{u,i}$ the respective local strengths. Crack propagation was simulated by a linear energy criterion

$$\frac{G_I}{G_{Ic}} + \frac{G_{II}}{G_{IIc}} = 1. \tag{12}$$

From Fig. 6 it is shown that the area of the triangle $0–\sigma_{um,i}–w_{um,i}$ corresponds to the energy released in each mode (G_i, $i = I, II$) during mixed-mode loading. Eqs. (11) and (12) can be written exclusively as a function of relative displacements, considering the relation between stresses/relative displacements as well as the one involving energies/relative displacements. This procedure allows defining the equivalent critical mixed-mode displacements corresponding to damage onset ($w_{om} = \sqrt{w_{om,I}^2 + w_{om,II}^2}$) and crack growth ($w_{um} = \sqrt{w_{um,I}^2 + w_{um,II}^2}$) under mixed-mode loading. These quantities are used to determine a damage

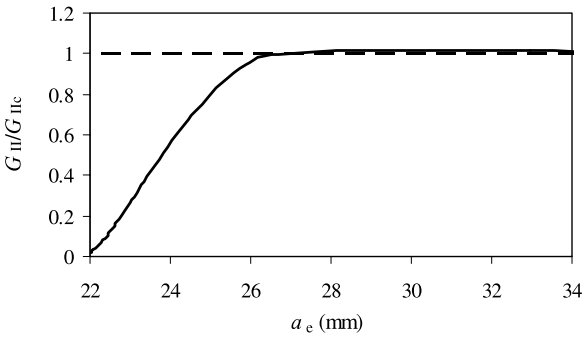

Fig. 7 – Numerical *R* curve of the ELS test.

parameter whose evolution is responsible for stress and stiffness decrease during loading. The cohesive zone model is detailed in de Moura et al. (2006).

Typical values of local strength $\sigma_{u,II} = 51.6$ MPa (Turner et al., 2001) and mode II toughness $G_{IIc} = 2.43$ N/mm (Feng et al., 2000) were used in the numerical analysis. Fig. 7 shows the plotting of the *R* curve normalized by the inputted toughness G_{IIc} in the cohesive model. As can be concluded, the inputted G_{IIc} is well captured in the plateau of the *R* curve, which demonstrates that the proposed data reduction scheme (Section 3) is valid to evaluate fracture toughness in bone. Consequently, the method will be applied in the next section to experimental data.

5. Results and discussion

Fig. 8 presents a typical load–displacement curve obtained in the experiments as well as the respective *R* curve determined by means of the procedure described in Section 3. The increase in the energy release rate observed in the ascending part of the *R* curve reflects the FPZ development. This phenomenon induces material softening which leads to stiffness reduction and gradual failure. When the FPZ is completely developed a self-similar crack growth takes place, i.e., the crack propagates with a constant FPZ size ahead of its tip. This leads to a plateau on the *R* curve which defines the material fracture toughness under pure mode II. An additional advantage of this procedure is related to the fact that *R* curves allow measurement of critical fracture energy during self-similar crack growth, independently of spurious problems related to pre-crack fabrication. Effectively, a blunt pre-crack induces an artificial initial increase of fracture energy followed by a plateau that provides the evaluation of material toughness (Morais et al., 2010).

A resume of the experimental results is presented in Table 2. The elastic longitudinal modulus (E_L) was measured for each specimen, since it is fundamental to calculate the fracture energy (Eq. (10)). The values of G_{IIc} were captured from the plateau of the *R* curves. An average value of $G_{IIc} = 2.65$ N/mm was obtained with a coefficient of variation of 7.8%, which can be considered reasonable for a biological material.

In order to verify if the proposed data reduction scheme is able to reproduce accurately the material fracture energy,

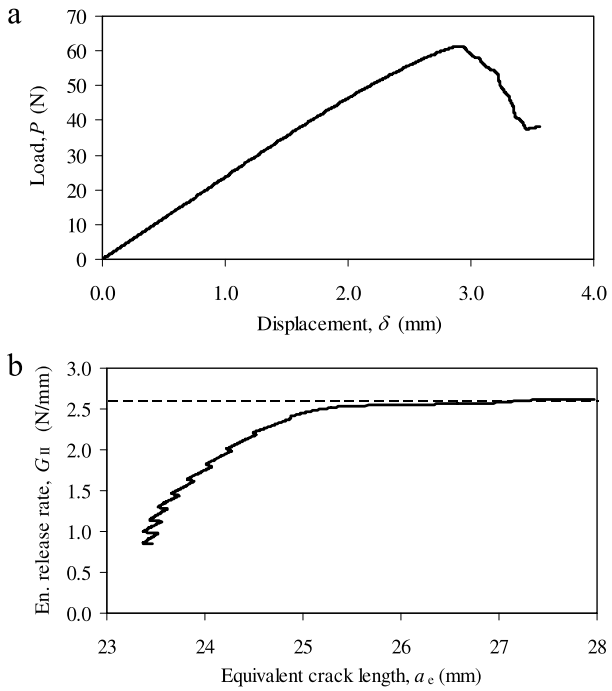

Fig. 8 – Typical load–displacement curve (a) and corresponding *R* curve (b) of the ELS test.

Table 2 – Resume of experimental results.

Specimen	E_L (GPa)	G_{IIc} (N/mm)
1	18.2	2.55
2	19.2	2.65
3	20.3	2.45
4	18.8	2.90
5	19.1	2.38
6	19.9	2.64
7	17.2	2.85
8	15.7	2.75
9	17.8	2.95
10	17.1	2.40
Average	18.3	2.65
CoV (%)	7.7	7.8

the specimen whose results are presented in Fig. 8 was numerically simulated. The value given by the plateau ($G_{IIc} = 2.64$ N/mm) was inputted in the numerical model and the resulting load–displacement curve was compared with the experimental one. Fig. 9(a) shows the good agreement obtained when a local strength of $\sigma_{u,II} = 65$ MPa was used. Additionally, it was observed that a cohesive zone with a constant length of approximately 3.0 mm (Fig. 9(b)) reproducing the FPZ is obtained during propagation, for a certain extent of equivalent crack growth. After that, confinement of the cohesive zone takes place thus inducing a spurious increase of measured fracture energy. This means that the proposed geometry is adequate to bone fracture characterization under pure-mode II loading since self-similar crack growth conditions arise for a given extent of crack propagation.

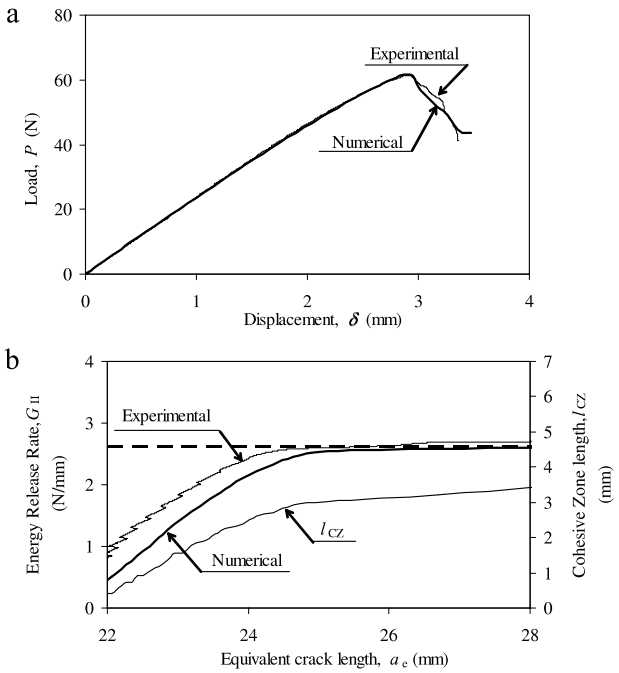

Fig. 9 – Comparison between the numerical and experimental (a) load–displacement curves and (b) the corresponding R curves.

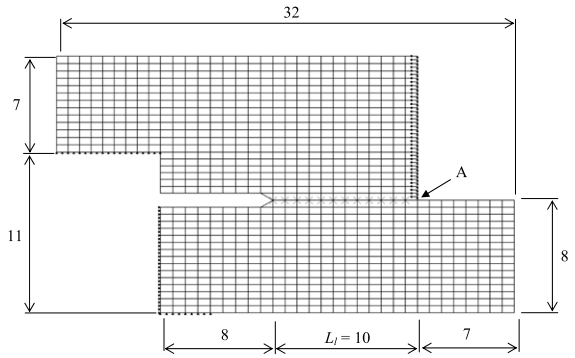

Fig. 10 – Compact shear test. Diagonal crosses along the crack path indicate the presence of cohesive elements. Dimensions are in mm.

6. Other test methods

In order to compare the ELS testing method with others proposed in the literature, numerical analyses were performed considering the same material properties used in this study. Therefore, the compact shear test (Norman et al., 1995) and the four-point bending test considering single-edge notched specimens (Zimmermann et al., 2009) were numerically simulated using the above described cohesive mixed-mode damage model.

6.1. *Compact shear test*

Fig. 10 shows the mesh used to simulate the compact shear test (CST). The loading, boundary conditions and specimen geometry comply with the test performed by

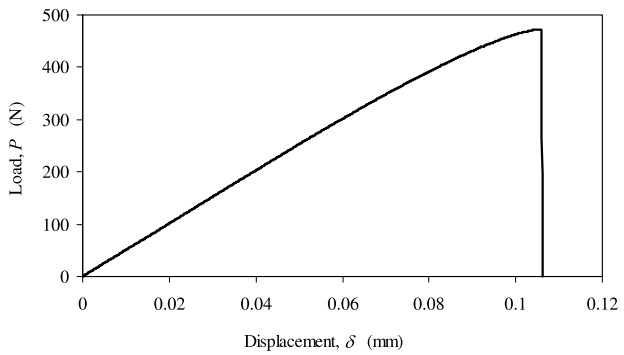

Fig. 11 – Load–displacement curve of CST.

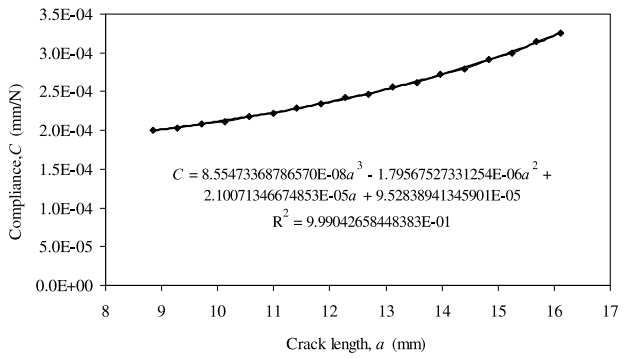

Fig. 12 – Compliance calibration of the CST, $C = f(a)$.

Norman et al. (1995). It was verified that softening occurs not only in the vicinity of the crack tip but also in the cohesive elements located near to the applied load (point A in Fig. 10). Additionally, a sudden failure was observed (Fig. 11) which hindered the establishment of compliance calibration during self-similar crack growth. In order to overcome this difficulty the compliance calibration was performed numerically considering several initial crack lengths. A cubic polynomial was fitted to the curve $C = f(a)$ with good correlation (Fig. 12). Afterwards, the current compliance during fracture test simulation is used to obtain an equivalent crack length $a_e = f(C)$, solving the adjusted cubic polynomial using the Matlab® software. This procedure allows the attainment of a normalized R curve, $G_{II}/G_{IIc} = f(a_e)$, using Eq. (1) and performing the derivative of the relation $C = f(a)$. The normalized R curve (Fig. 13) presents a rising trend without any plateau and shows that the inputted fracture energy G_{IIc} is not captured. This is explained by the fact that self-similar crack growth conditions are not satisfied with these specimen dimensions. In fact, it was observed that all the cohesive elements are under softening in the increment just before catastrophic failure, which means that the ligament length is insufficient to satisfy the conditions of accurate fracture energy measurement. In order to confirm this statement, a second simulation considering a theoretical specimen with a double ligament length (i.e., $L_l = 20$ mm) was performed. In this case, the fracture process zone did not attain all the ligament length before failure and the resulting R curve presents a clear plateau with a small difference relative to the

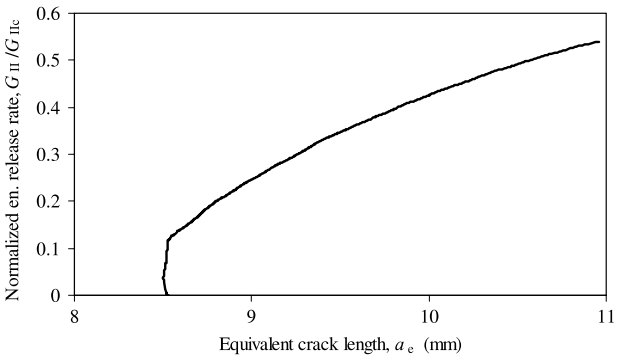

Fig. 13 – Normalized R curve obtained for CST test.

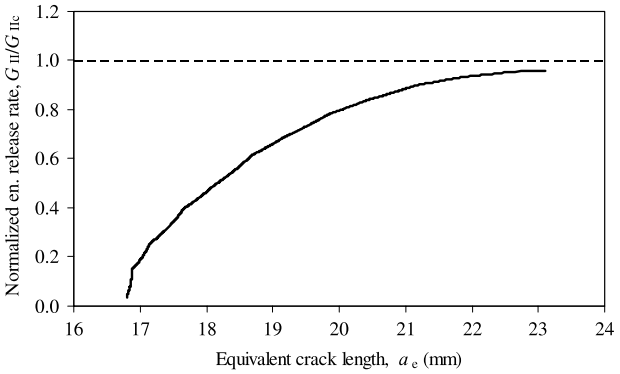

Fig. 14 – Normalized R curve obtained for CST test for $L_1 = 20$ mm.

inputted G_{IIc} (Fig. 14). This small discrepancy can be explained by the circumstance that some energy is dissipated close to point A in Fig. 10.

This numerical analysis leads to the conclusion that this test presents some difficulties which concern the accurate measurement of fracture energy under pure mode II loading. At least, longer specimens should be used to guarantee reliable estimation of bone fracture energy.

6.2. *Four-point bending test*

Zimmermann et al. (2009) proposed the asymmetric four-point bending test considering single-edge notched specimens. Pure mode II conditions arise when the pre-crack is aligned with the centerline of the rig, since in this case the bending moment vanishes and only a shear force is applied. Fig. 15(a) illustrates the mesh used considering loading and supporting cylinders. The load is applied to the central upper cylinder which is rigidly connected to the other upper cylinders by kinematic constraints, thus simulating a rigid beam. Fig. 15(b) highlights the fracture development observed numerically for the conditions stipulated for mode II fracture characterization. The first aspect observed during simulations is that the development of the FPZ at crack initiation is under mixed-mode and not under pure mode II loading. Fig. 16(a) represents the profiles of stress components (σ_I and σ_{II}) along the crack path ahead of the crack tip. It can be observed that an important value of the mode I stress component (even higher than mode II) exists at the crack tip just before softening occurs (linear elastic domain). Ahead of the crack tip (approximately 1 mm) the mode II component presents an almost constant profile and mode I practically vanishes. Fig. 16(b) shows the profile of stress components just before crack starting advance, i.e., inside the FPZ which has a length similar to the one obtained in the ELS test, i.e., approximately 3.0 mm (Fig. 9(b)). It can be clearly observed (Fig. 16(b)) that the mode I stress component presents an almost constant trend being predominant till approximately 2.3 mm ahead of the crack tip. This means that FPZ is clearly under mixed-mode conditions, thus affecting the measured value of mode II toughness. This aspect can also be observed in Fig. 17 which presents a detail of the crack tip just before crack propagation. Effectively, the observed overture clearly shows an important opening relative displacement (mode I) due to damage development in the FPZ for the increment just before crack starting advance. The darker region represents the zone where the mode I stress component is more pronounced which also highlights the importance of mode I loading in the FPZ. As a result, the R curve (Fig. 18) presents a monotonic rising trend depicting the changing of mode-mixity as the crack grows. Consequently, the conditions of crack propagation even at its initiation do not fulfill the ones required for pure mode II fracture characterization.

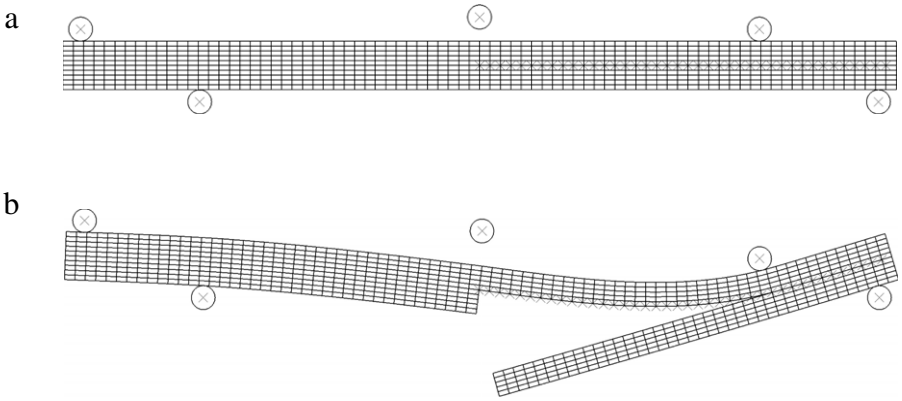

Fig. 15 – (a) Mesh used and (b) fracture development of the asymmetric four-point bending test.

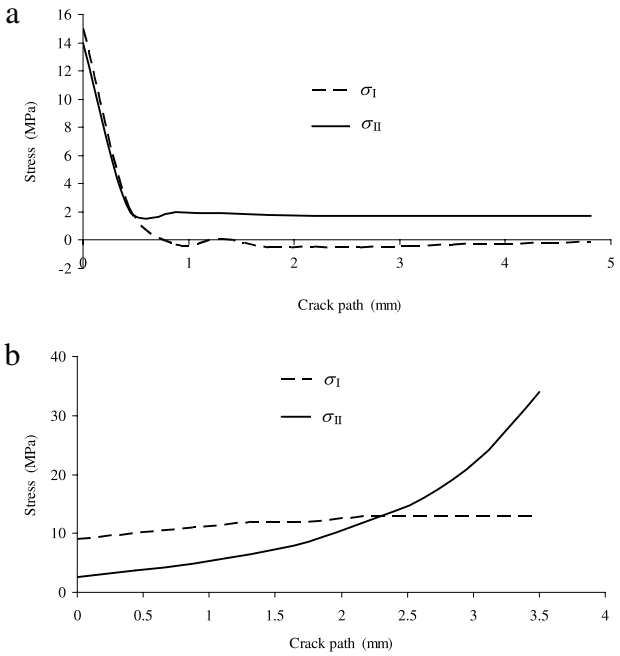

Fig. 16 – Stress profiles along the crack path ahead of the crack-tip for the FPB test just before (a) damage onset and (b) crack starting advance.

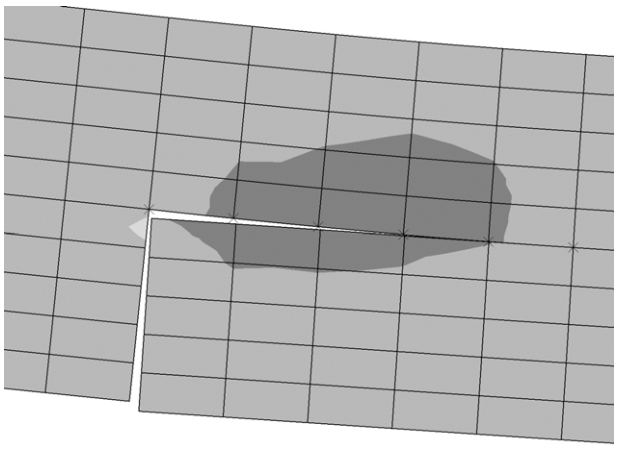

Fig. 17 – Detail showing the relative displacements and mode I stresses (darker region) in the FPZ prior to crack propagation.

7. Conclusions

In this work fracture characterization of bone under pure mode II loading was studied. The end loaded split test was applied to young bovine cortical bone. Experimental tests were performed using specimen dimensions issued from a recent numerical study. The experimental praxis during the execution of ELS tests revealed that the crack frequently deviates from specimen mid-plane during its growth. Hence, in order to overcome this drawback a slight longitudinal groove has been machined in both sides of the specimen, thus compelling crack advance to occur along the longitudinal axis. During propagation in pure mode II, crack tends to grow closed, which makes it difficult to identify its tip. Thus, an equivalent crack method which does not require crack length monitoring during its growth was used to resolve this experimental difficulty. The method is based on specimen compliance which is used to estimate the equivalent crack length. Additionally, the proposed procedure presents an additional advantage since it accounts indirectly for the presence of the FPZ. The data reduction scheme was validated by means of a numerical analysis using a cohesive zone model, and subsequently applied to experimental load–displacement curves. Consistent results were obtained from a series of ten tested specimens which demonstrates that the end loaded split test considering the proposed dimensions is adequate to determine fracture toughness of bone under pure mode II loading.

Alternative tests proposed in the literature for bone fracture characterization under mode II loading were also duly analyzed numerically. It was concluded that both of them present some limitations regarding the accurate determination of fracture toughness under pure mode II loading. These results emphasize the interest of the proposed ELS and data reduction scheme in the field.

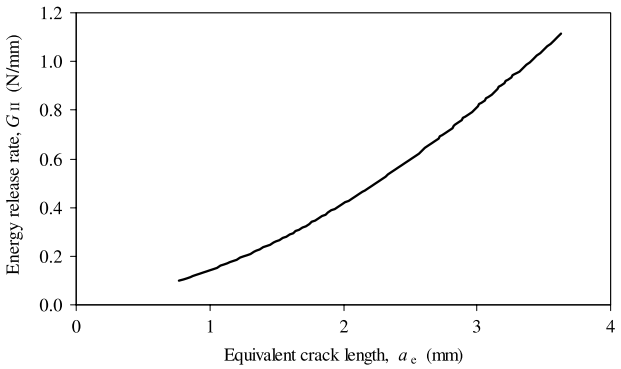

Fig. 18 – Normalized R curve obtained for CST test.

Acknowledgment

The authors acknowledge the Portuguese Foundation for Science and Technology (FCT) for the conceded financial support through the research project PDTC/EME/PME/71273/2006.

REFERENCES

de Moura, M.F.S.F., Silva, M.A.L., de Morais, A.B., Morais, J.J.L., 2006. Equivalent crack based mode II fracture characterization of wood. Engineering Fracture Mechanics 73, 978–993.

de Moura, M.F.S.F., Silva, M.A.L., Morais, J.J.L., de Morais, A.B., Lousada, J.J.L., 2009. Data reduction scheme for measuring G_{IIc} of wood in End-Notched Flexure (ENF) tests. Holzforschung 63, 99–106.

de Moura, M.F.S.F., Dourado, N., Morais, J.J.L., 2010a. Crack equivalent based method applied to wood fracture characterization using the single edge notched-three point bending test. Engineering Fracture Mechanics 77, 510–520.

de Moura, M.F.S.F., Dourado, N., Morais, J.J.L., Pereira, F.A.M., 2010b. Numerical analysis of the ENF and ELS tests applied to mode

II fracture characterization of cortical bone tissue. Fatigue & Fracture of Engineering Materials & Structures 34, 149–158.

Dourado, N., de Moura, M.F.S.F., Morais, J.J.L., 2011. A numerical study on the SEN-TPB test applied to mode I wood fracture characterization. International Journal of Solids and Structures 48, 234–242.

Feng, Z., Rho, J., Han, S., Ziv, I., 2000. Orientation and loading condition dependence of fracture toughness in cortical bone. Materials Science and Engineering: C 11, 41–46.

Hernandez, C.J., Beaupré, G.S., Keller, T.S., Carter, D.R., 2001. The influence of bone volume fraction and ash fraction on bone strength and modulus. Bone 29, 74–78.

Martin, R.B., Burr, D.B., Sharkey, N.A., 1998. Skeletal Tissue Mechanics. Springer-Verlag, New York, ISBN: 0-387-98474-7.

Morais, J.J.L., de Moura, M.F.S.F., Pereira, F.A.M., Xavier, J., Dourado, N., Dias, M.I.R., Azevedo, J.M.T., 2010. The double cantilever beam test applied to mode I fracture characterization of cortical bone tissue. Journal of the Mechanical Behavior of Biomedical Materials 3, 446–453.

Nalla, R.K., Kinney, J.H., Ritchie, R.O., 2003. Mechanistic fracture criteria for the failure of human cortical bone. Nature Materials 2, 164–168.

Norman, T.L., Vashishtht, D., Burr, D.B., 1995. Fracture toughness of human bone under tension. Journal of Biomechanics 28, 309–320.

Norman, T.L., Nivargikar, V., Burr, D.B., 1996. Resistance to crack growth in human cortical bone is greater in shear than in tension. Journal of Biomechanics 29, 1023–1031.

Phelps, J.B., Hubbard, G.B., Wang, X., Agrawal, C.M., 2000. Microstructural heterogeneity and the fracture toughness of bone. Journal of Biomedical Materials Research 51, 735–741.

Turner, C.H., Wang, T., Burr, D.B., 2001. Shear strength and fatigue properties of human cortical bone determined from pure shear tests. Calcified Tissue International 69, 373–378.

Wang, X., Shen, X., Li, X., Agrawal, M., 2002. Age-related changes in the collagen network and toughness of bone. Bone 31, 1–7.

Wang, Y., Williams, J.G., 1992. Corrections for mode II fracture toughness specimens of composite materials. Composites Science and Technology 43, 251–256.

Zimmermann, E.A., Launey, M.E., Barth, H.D., Ritchie, R.O., 2009. Mixed-mode fracture of human cortical bone. Biomaterials 30, 877–5884.

Zimmermann, E.A., Launey, M.E., Ritchie, R.O., 2010. The significance of crack-resistance curves to the mixed-mode fracture toughness of human cortical bone. Biomaterials 31, 5297–5305.

Zioupos, P., 1998. Recent developments in the study of failure of solid biomaterials and bone: fracture and pre-fracture toughness. Materials Science and Engineering: C 6, 33–40.